Chemical Science

ROYAL SOCIETY OF CHEMISTRY

EDGE ARTICLE

View Article Online
View Journal | View Issue

Cite this: *Chem. Sci.*, 2024, **15**, 19764

All publication charges for this article have been paid for by the Royal Society of Chemistry

Received 14th October 2024
Accepted 11th November 2024

DOI: 10.1039/d4sc06989g

rsc.li/chemical-science

Understanding the formation of nitrate from nitrogen at the interface of gas–water microbubbles†

Sandeep Bose, Yu Xia* and Richard N. Zare *

Water microbubbles containing Fe^{2+} ions have been found to efficiently transform nitrogen (N_2) to nitrate (NO_3^-) by initiating Fenton's reaction at the gas–water interface. Herein, we elucidate the mechanism of the formation of nitrate (NO_3^-) from nitrogen (N_2) at the microbubble interface. Several experimental studies were conducted to identify the intermediates formed during the conversion. Our investigation shows the formation of $H_2N_2O_2$, NO, NO_2, and NO_2^- intermediates before yielding NO_3^- as the final product. Density functional theory (DFT) calculations provide additional support to our observation by providing insights into the energy profiles of the reaction intermediates. We believe that this work not only provides valuable insight into the abiotic nitrogen fixation in microbubbles but also helps in suggesting the modification of parameters to create a more reactive interface that leads to the enhanced production of nitric acid (HNO_3).

Introduction

Atmospheric nitrogen (N_2) fixation is essential for life on Earth because it converts non-reactive N_2 into a reactive form that is suitable for crops and supports their growth.[1] Nitrate (NO_3^-) is one of the nitrogen fixation products that is widely used to manufacture fertilizers.[2] Additionally, NO_3^- is employed as a vital source of nitrogen in the food processing industry and the manufacturing of plastic and medicinal products.[3] Traditionally, NO_3^- is prepared from the catalytic oxidation of ammonia (NH_3).[4] The method suffers from the use of NH_3 which is generally prepared from the Haber–Bosch process. The process involves the use of fossil fuel and the release of large quantities of carbon dioxide (CO_2).[4] Intense research has been directed toward the goal of producing NO_3^- in a more eco-friendly way.[3]

Recently, reactions in water microdroplets and microbubbles have been explored as an alternative approach owing to a significant enhancement in the reaction rates and formation of unexpected products.[5–17] An exceptional electric field strength ($\sim 10^9$ V m^{-1}),[18–21] the lack of three-dimensional solvation,[22,23] the orientation of molecules at the interface,[24–26] evaporation,[27] and pH[28] are several factors that drive redox reactions at the air–water interface. Taking advantage of these factors, Bose, Mofidfar, and Zare have shown that NO_3^- can be successfully prepared by passing N_2 microbubbles through water in the presence of Fe^{2+}.[29] The presence of ferrous ions stimulates $OH^\bullet$ production at the microbubble interface by initiating Fenton's reaction as follows:[30,31]

$$Fe^{2+} + H_2O_2 \rightarrow Fe^{3+} + OH^\bullet + OH^- \quad (1)$$

The $OH^\bullet$ produced from Fenton's reaction activates the N_2 molecule which undergoes a series of transformations to form HNO_3 as the final product. Surprisingly, the transformations occur at room temperature and ambient pressure. Additionally, the process does not require any external electric field or radiation, and hence opens up the possibility for an eco-friendly production of HNO_3.

Experimentally, the authors have confirmed that N_2 oxidation takes place at the gas–water interface of a microbubble.[29] To ensure the necessity of microbubbles for the transformation, the author simply purged the solution with N_2 to create larger bubbles. No NO_3^- formation was noticed in case of larger bubbles which suggests the requirement of microbubbles for the conversion. Although the final product was analysed and quantified, the exact mechanism for that conversion was not established. The current work involves the understanding of the reaction pathways for the formation of NO_3^- from N_2. We have performed several experiments to recognize the intermediates formed during the process. Based on these identifications, we propose a possible reaction leading to intermediate formation. Finally, we tried to connect all the possible reactions as a sequence of continuous steps that occur to yield the final product. To validate our experimental observations, density functional theory (DFT) calculations were employed. DFT studies unravel the reaction pathways involving the

Department of Chemistry, Stanford University, CA 94305, USA. E-mail: zare@stanford.edu

† Electronic supplementary information (ESI) available. See DOI: https://doi.org/10.1039/d4sc06989g

experimentally identified intermediates and show the feasibility of the transformation.

Experimental

The reaction system which was used for NO_3^- production consists of an air stone submerged in a beaker of aqueous $FeSO_4$ (50 μM) solution. The air stone is a cylindrical porous mineral bubbler used to create microbubbles. The beaker is placed inside an ultrasonic bath along with a temperature controller. The air stone is connected to the N_2 gas supply. When N_2 gas (50 psi) is allowed to pass through the air stone, it produces microbubbles of N_2 in the solution.[29] An air stone is a porous material that is used to diffuse gas bubbles into water. The air stones (Guangzhou Zhushi Aquarium Co., Ltd, ASC-999) are manufactured from quartz sand that has been sintered in a fixed mold. The size of the output bubble depends upon the input gas pressure and the porosity of the air stone. The air stone we employed for our experiment has a porosity of 11%. Through the use of a high-speed camera, we found the average diameter of the microbubbles is ~530 μm and the average flux of the output bubble is ~120 microbubbles per second for a gas pressure of 50 psi. We employed ultrasonication along with bubbling to further split microbubbles to cause them to have smaller sizes. A temperature controller was used to prevent an increase in temperature. However, evaporation still occurs over time, and water was added to the container to maintain the same level of water. An activated carbon filter was inserted in the gas flow to remove any nitrogen oxide impurities present.

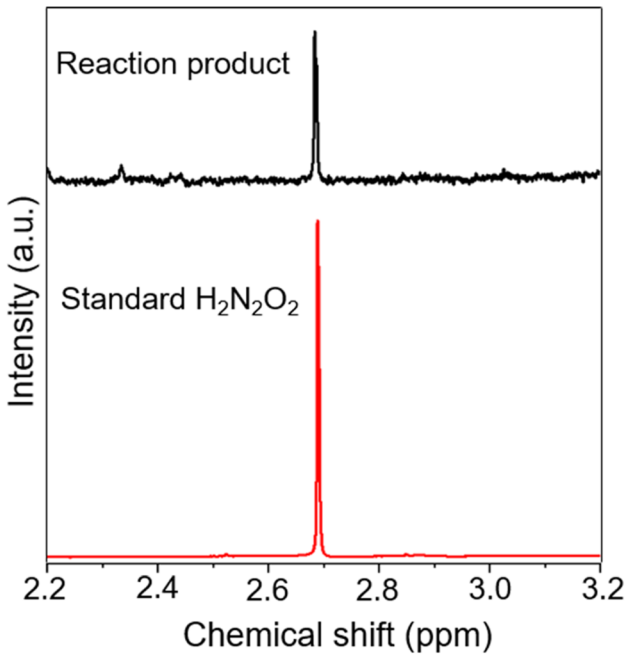

Fig. 1 Comparison of the ^{1}H-NMR spectra of the reaction product after 30 min of microbubbling and the standard $H_2N_2O_2$ solution.

Results and discussion

Before identification of intermediates, we detected H_2O_2 formation as it is important for Fenton's reaction to generate $OH^{\bullet}$ for N_2 activation. The quantification of H_2O_2 was done using a potassium titanium oxalate based spectrophotometric method[29] which shows a continuous increase in H_2O_2 production with bubbling (Fig. S1†). The N_2 activation leading to NO_3^- as the final product was confirmed by using the method reported by Bose, Mofidfar, and Zare[29] which shows a steady increase in NO_3^- yield with bubbling time (Fig. S2†).

For the identification of intermediates involved in NO_3^- formation, the ^{1}H-NMR spectrum of the reaction solutions was measured after 30 min of bubbling. The NMR spectrum shows a chemical shift of 2.69 (Fig. 1) which can be attributed to the formation of hyponitrous acid ($H_2N_2O_2$).[32] The generation of $H_2N_2O_2$ in the solution was confirmed by measuring the NMR of a standard $H_2N_2O_2$ solution which shows a peak at the same position. Thus, it can be concluded that N_2 is activated by the *in*

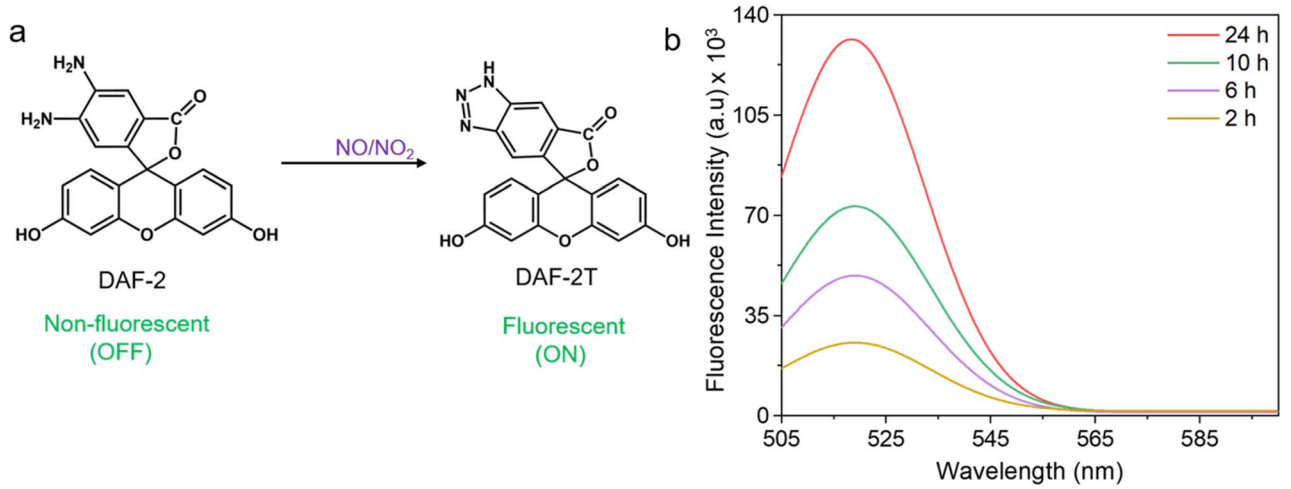

Fig. 2 (a) Schematic representation of the conversion of non-fluorescent DAF-2 to fluorescent DAF-2T in the presence of NO/NO_2 present in the medium. (b) Change in fluorescence intensity of the DAF-2 containing N_2-bubbling solution with time.

situ generated OH˙ from Fenton's reaction which oxidizes N_2 to yield $H_2N_2O_2$ in a sequence of steps. The reactions can be shown as follows:

$$N_2 + H^{\cdot} \rightarrow N_2H^{\cdot} + OH^{\cdot} \rightarrow HN_2OH + OH^{\cdot} \rightarrow {}^{\cdot}N_2OH + H_2O + OH^{\cdot} \rightarrow H_2N_2O_2 + H_2O \quad (2)$$

Other important intermediates identified from the micro-bubbled solution are nitric oxide (NO˙) and nitrogen dioxide ($NO_2^{\cdot}$). To obtain direct evidence of NO and NO_2 in the solution, we employed diaminofluorescein (DAF-2) as a fluorescent indicator. DAF-2 itself is a weakly fluorescent molecule which in the presence of NO˙ and oxygen undergoes a chemical transformation to yield a highly green fluorescent triazole form known as DAF-2T (Fig. 2a).[33] The reaction mechanism is proposed to involve the formation of nitrous anhydride (N_2O_3) which is produced as follows:[34]

$$2NO^{\cdot} + O_2 \rightarrow 2NO_2^{\cdot} \quad (3)$$

$$NO^{\cdot} + NO_2^{\cdot} \rightarrow N_2O_3 \quad (4)$$

The *in situ* produced N_2O_3 reacts with the vicinal diamines of DAF-2 to form the triazole ring compound (DAF-2T).

To check the existence of NO˙ and $NO_2^{\cdot}$ in our sample, we added 5 mM DAF-2 in DMSO to the microbubbled solution. As the N_2-bubbling time is increased, we observe an increase in the fluorescence intensity (λ_{ex} = 495 nm, λ_{em} = 515 nm). The fluorescence intensity of DAF-2 is weak, and it shows substantial enhancement in fluorescence upon N_2-bubbling for 24 h (Fig. S3†). This suggests that N_2O_3 concentration increases in the solution, and the *in situ* generated N_2O_3 reacts with the DAF-2 present in the solution to give DAF-2T which enhances the fluorescence (Fig. 2b).[33] Thus, it can be concluded that both NO˙ and $NO_2^{\cdot}$ are generated in the microbubbles during the reaction. From eqn (2) we showed that the first steps of N_2 activation occurs *via* $H_2N_2O_2$ formation. The $H_2N_2O_2$ formed possibly reacts with the OH˙ generated in the system, to produce NO˙. The reaction can be written as follow:

$$H_2N_2O_2 + 2OH^{\cdot} \rightarrow 2NO^{\cdot} + 2H_2O \quad (5)$$

In living cells, NO˙ reacts with O_2 to form $NO_2^{\cdot}$ as shown in eqn (3). However, in our case, the microbubbles were produced using N_2 as feed gas and the system lacks oxygen to produce $NO_2^{\cdot}$. Thus, a possible way by which $NO_2^{\cdot}$ could be produced from NO˙ is shown by the following reaction:

$$NO^{\cdot} + OH^{\cdot} \rightarrow HNO_2 \quad (6)$$

$$HNO_2 + OH^{\cdot} \rightarrow NO_2^{\cdot} + H_2O \quad (7)$$

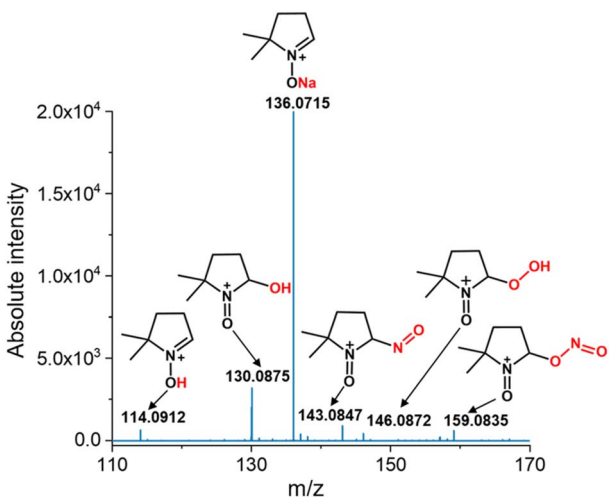

Fig. 3 Mass spectrum of the reactive oxygen species (ROS) and reactive nitrogen species (RNS) captured by DMPO in the N_2-micro-bubbled solution.

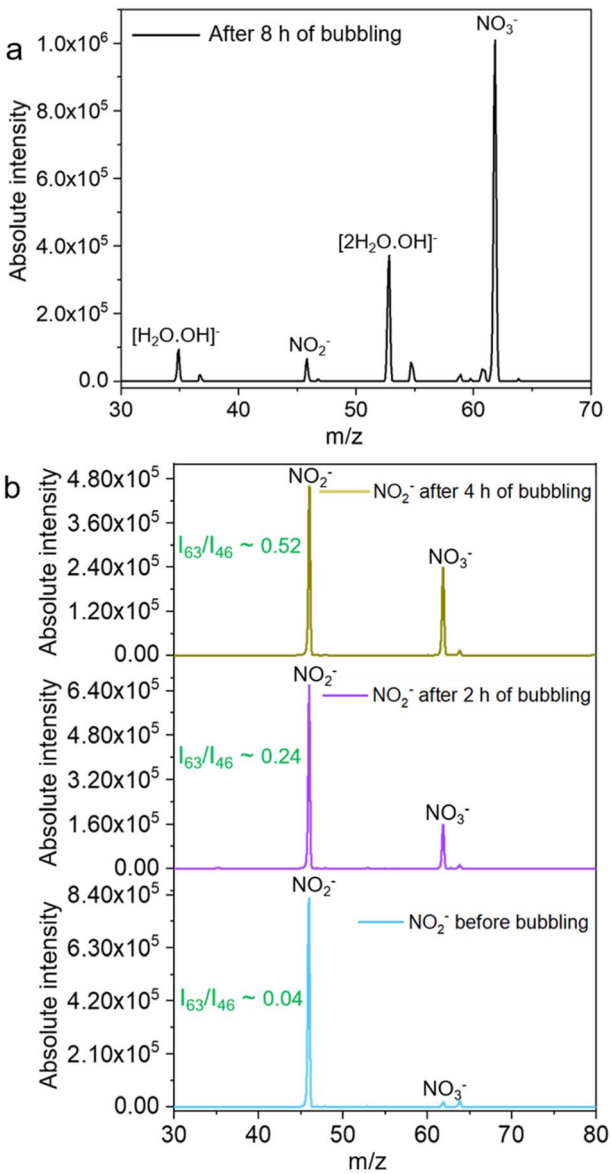

Fig. 4 (a) Mass spectrum of the N_2-bubbled sample after 8 h. The mass spectrum shows a tiny peak of NO_2^- along with NO_3^-. (b) A comparison of the mass spectrum of the control NO_2^- (20 μM) before bubbling and after bubbling for 2 h and 4 h.

Additionally, we employed the spin trap, 5,5-dimethyl-1-pyrroline-*N*-oxide (DMPO), to capture the reactive oxygen species (ROS) and reactive nitrogen species (RNS) as shown previously by Song *et al.*[35] During the microbubbling experiment, DMPO (2 mM) was added to the solution and bubbling was continued for a sufficiently longer time to capture any radical species generated in the solution. Finally, the solution was analyzed using mass spectrometry (Orbitrap MS). DMPO captures ROS such as $OH^{\bullet}$ and $OOH^{\bullet}$ which were characterized by the formation of DMPO-OH (*m*/*z* 130.0875) and DMPO-OOH (*m*/*z* 146.0872). The $OH^{\bullet}$ captured by DMPO was generated from Fenton's reaction in the presence of Fe^{2+} in the solution whereas the $OOH^{\bullet}$ detected possibly results from the catalytic regeneration of Fe^{2+} from Fe^{3+} at the gas–water interface as follows:

$$Fe^{3+} + H_2O_2 \rightarrow Fe^{2+} + HO_2^{\bullet} + H^+ \quad (8)$$

In addition, we observed features at *m*/*z* 114.0912 and 136.0715 corresponding to DMPO-H and DMPO-Na, respectively. Apart from ROS, we also observed RNS such as $NO^{\bullet}$ and $NO_2^{\bullet}$ which were detected as DMPO-NO (*m*/*z* 143.0847) and DMPO-NO_2 (*m*/*z* 159.0835) in the mass spectrum (Fig. 3). As both the $NO^{\bullet}$ and $NO_2^{\bullet}$ are radical species, they form a covalent bond at the C(sp^2)-2 position of the DMPO resulting in the formation of DMPO-NO and DMPO-NO_2. From both the fluorescence measurement and mass spectral interpretation we concluded that $NO^{\bullet}$ and $NO_2^{\bullet}$ intermediates are produced during the bubbling.

When the mass spectrum of the N_2-microbubbled sample was recorded after 4 h, it showed a feature at *m*/*z* 46 due to NO_2^- (negative ion mode) along with the product peak of NO_3^- at *m*/*z* 63. This suggests that NO_2^- is formed during the reaction and possibly works as an intermediate to obtain NO_3^- as the final product (Fig. 4a). To confirm NO_3^- conversion occurs *via* NO_2^-, we externally prepare a NO_2^- solution of known concentration (20 μM) and the solution was microbubbled. When the mass spectra were recorded (LTQ MS), we observed an increase in the NO_3^- intensity with increasing bubbling time (Fig. 4b). This suggests that the NO_2^- generated in the microbubble is involved in NO_3^- formation which possibly occurs *via* oxidation in the presence of $OH^{\bullet}$. Because N_2 as a feed gas can cause NO_3^- formation, we employed argon gas for this particular experiment to create microbubbles. Also, NO_2^- in aqueous solution when kept for long and exposed to light undergoes slow oxidation to NO_3^-. To check NO_2^- oxidation in aqueous solution we kept the solution without bubbling for 2 h and 4 h and measured the mass spectrum. We did not observe any oxidation of the NO_2^- solution when kept without bubbling (Fig. S4†). This suggests that the NO_2^- oxidation to NO_3^- takes place only in microbubbles. As eqn (7) shows that NO_2^- reacts with $OH^{\bullet}$ to form NO_2, so we believe the conversion of NO_2^- to NO_3^- occurs *via* NO_2 generation in the microbubbles as follows:

$$HNO_2 + OH^{\bullet} \rightarrow NO_2^{\bullet} + H_2O \quad (9)$$

$$NO_2^{\bullet} + OH^{\bullet} \rightarrow HNO_3 \quad (10)$$

$$N_2^{\bullet} \rightarrow H_2N_2O_2 \rightarrow 2NO + 2H_2O \rightarrow 2HNO_2 + 2H_2O \rightarrow 2NO_2 + 4H_2O \rightarrow 2HNO_3 + 4H_2O \quad (11)$$

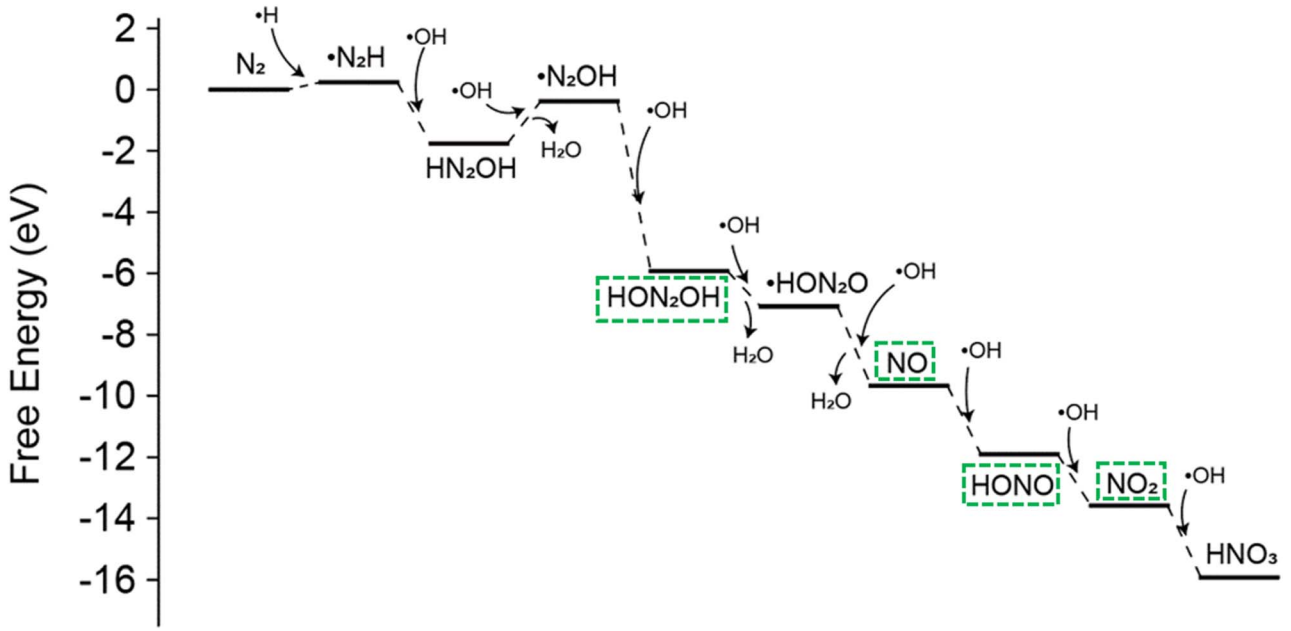

Fig. 5 DFT calculation showing the energy profile of the intermediates involved in the N_2 oxidation to NO_3^- in the microbubbles. The experimentally identified intermediates are shown in green color dashed rectangles.

From all the above experiments we identified that $H_2N_2O_2$, $NO^{\bullet}$, $NO_2^{\bullet}$, and NO_2^- are the intermediates formed when N_2 is converted to NO_3^- in the microbubbles. Based on our experimental evidence and combining eqn (1)–(9) we suggest the oxidation of N_2 to NO_3^- by $OH^{\bullet}$ activation takes place through a series of sequential transformations as follows:

To validate the proposed reaction pathway for the conversion of N_2 to NO_3^- *via* the gas–water interface, we conducted further investigations into the reaction mechanism using DFT calculations. The designed interfacial reaction system typically includes active radicals, such as hydrogen and hydroxyl radicals. As we previously reported, hydrogen radicals at the gas–water interface can activate nitrogen molecules, allowing them to react with other radicals.[36] In subsequent steps, the nitrogen–nitrogen triple bond (N≡N) breaks progressively, eventually leading to the formation of nitrate through oxidation (Fig. 5). Compared to the high activation energy of 0.95 eV for O_2 oxidation, the further oxidation of $NO^{\bullet}$ by $OH^{\bullet}$ to form HNO_3 proceeds without an energy barrier.

We do not claim this is the only pathway through which NO_3^- is formed, and it is possible that the reaction might involve some unknown intermediates and reaction pathways that we failed to identify. But the experimental and theoretical evidence we have found points to the reaction pathways we have presented as being operative.

Conclusions

In summary, we have experimentally detected different intermediates namely $H_2N_2O_2$, $NO^{\bullet}$, $NO_2^{\bullet}$, and NO_2^- produced in microbubbles during the conversion of N_2 to NO_3^-. ^{1}H-NMR spectroscopy was utilized to identify $H_2N_2O_2$. DAF-2 was employed to confirm the existence of $NO^{\bullet}$ and $NO_2^{\bullet}$ in the microbubbled solution spectrophotometrically. In addition, DMPO-based spin trap experiments captured the RNS ($NO^{\bullet}$ and $NO_2^{\bullet}$) in the mass spectrum. The presence of NO_2^- along with NO_3^- was observed in the mass spectrum. DFT calculations support our experimental evidence by providing insights into the energy profile of the reaction intermediates.

Data availability

The data supporting this article have been included as part of the ESI.†

Author contributions

S. B. performed most of the experiments, analysis, and drafting of the first version of the manuscript. Y. X. helped in the DFT calculation. R. N. Z., the principal investigator, proposed the project, supervised all co-authors, and completely revised the manuscript.

Conflicts of interest

There are no conflicts to declare.

Acknowledgements

S. B. would like to thank the Nehru-Fulbright program for the fellowship. We thank the Air Force Office of Scientific Research through the Multidisciplinary University Research Initiative (MURI) program (AFOSR FA9550-21-1-0170) for supporting this project.

Notes and references

1 N. Cherkasov, A. O. Ibhadon and P. Fitzpatrick, *Chem. Eng. Process. Process Intensif.*, 2015, **90**, 24–33.
2 2015–2032 Nitric Acid Market Analysis: Industry Market Size, Plant Capacity, Production, Operating Efficiency, Demand & Supply, Type, End-User Industries, Sales Channel, Regional Demand, Foreign Trade, Company Share, Manufacturing Process, Policy and Regulatory Landscape, 2024, **https://www.chemanalyst.com/industry-report/nitric-acid-market-615**.
3 Y. Tang, J. Dai, P. Zhang, G. Niu, Y. Duan and Y.-H. Tian, *ACS Sustainable Chem. Eng.*, 2024, **12**, 11319–11326.
4 US EPA, AP 42 Chapter 8.8 Nitric acid Production, **https://gaftp.epa.gov/ap42/ch08/s08/final/c08s08_feb1998.pdf**.
5 X. Song, Y. Meng and R. N. Zare, *J. Am. Chem. Soc.*, 2022, **144**, 16744–16748.
6 S. Jin, H. Chen, X. Yuan, D. Xing, R. Wang, L. Zhao, D. Zhang, C. Gong, C. Zhu, X. Gao, Y. Chen and X. Zhang, *JACS Au*, 2023, **3**, 1563–1571.
7 Y. B. Vogel, C. W. Evans, M. Belotti, L. Xu, I. C. Russell, L.-J. Yu, A. K. K. Fung, N. S. Hill, N. Darwish, V. R. Gonçales, M. L. Coote, K. Swaminathan Iyer and S. Ciampi, *Nat. Commun.*, 2020, **11**, 6323.
8 J. K. Lee, D. Samanta, H. G. Nam and R. N. Zare, *Nat. Commun.*, 2018, **9**, 1562, DOI: **10.1038/s41467-018-04023-z**.
9 A. Nandy, A. Kumar, S. Mondal, D. Koner and S. Banerjee, *J. Am. Chem. Soc.*, 2023, **145**, 15674–15679.
10 D. Satyabola, T. Ahuja, S. Bose, B. Mondal, P. Srikrishnarka, M. P. Kannan, B. K. Spoorthi and T. Pradeep, *J. Phys. Chem. C*, 2021, **125**, 10998–11006.
11 A. Ray Chowdhuri, B. K. Spoorthi, B. Mondal, P. Bose, S. Bose and T. Pradeep, *Chem. Sci.*, 2021, **12**, 6370–6377.
12 S. Bose, A. Chatterjee, S. K. Jenifer, B. Mondal, P. Srikrishnarka, D. Ghosh, A. R. Chowdhuri, M. P. Kannan, S. V Elchuri and T. Pradeep, *ACS Sustainable Chem. Eng.*, 2021, **9**, 4554–4563.
13 J. Ghosh and R. G. Cooks, *TrAC, Trends Anal. Chem.*, 2023, **161**, 117010.
14 S. Banerjee, E. Gnanamani, X. Yan and R. N. Zare, *Analyst*, 2017, **142**, 1399–1402.
15 X. Yan, R. M. Bain and R. G. Cooks, *Angew. Chem., Int. Ed.*, 2016, **55**, 12960–12972.
16 D. Zhang, J. Wang, H. Chen, C. Gong, D. Xing, Z. Liu, I. Gladich, J. S. Francisco and X. Zhang, *J. Am. Chem. Soc.*, 2023, **145**, 6462–6470.
17 B. K. Spoorthi, K. Debnath, P. Basuri, A. Nagar, U. V Waghmare and T. Pradeep, *Science*, 2024, **384**, 1012–1017.

18 D. Zhang, X. Yuan, C. Gong and X. Zhang, *J. Am. Chem. Soc.*, 2022, **144**, 16184–16190.
19 Z. Song, C. Liang, K. Gong, S. Zhao, X. Yuan, X. Zhang and J. Xie, *J. Am. Chem. Soc.*, 2023, **145**, 26003–26008.
20 H. Xiong, J. K. Lee, R. N. Zare and W. Min, *J. Phys. Chem. Lett.*, 2020, **11**, 7423–7428.
21 C. Zhu, L. N. Pham, X. Yuan, H. Ouyang, M. L. Coote and X. Zhang, *J. Am. Chem. Soc.*, 2023, **145**, 21207–21212.
22 L. Qiu, Z. Wei, H. Nie and R. G. Cooks, *Chempluschem*, 2021, **86**, 1362–1365.
23 Z. Wei, Y. Li, R. G. Cooks and X. Yan, *Annu. Rev. Phys. Chem.*, 2020, **71**, 31–51.
24 K. Inoue, M. Ahmed, S. Nihonyanagi and T. Tahara, *Nat. Commun.*, 2020, **11**, 5344.
25 G. R. Medders and F. Paesani, *J. Am. Chem. Soc.*, 2016, **138**, 3912–3919.
26 Z. Zhou, X. Yan, Y.-H. Lai and R. N. Zare, *J. Phys. Chem. Lett.*, 2018, **9**, 2928–2932.
27 G. Rovelli, M. I. Jacobs, M. D. Willis, R. J. Rapf, A. M. Prophet and K. R. Wilson, *Chem. Sci.*, 2020, **11**, 13026–13043.
28 H. Wei, E. P. Vejerano, W. Leng, Q. Huang, M. R. Willner, L. C. Marr and P. J. Vikesland, *Proc. Natl. Acad. Sci. U. S. A.*, 2018, **115**, 7272–7277.
29 S. Bose, M. Mofidfar and R. N. Zare, *J. Am. Chem. Soc.*, 2024, **146**, 27964–27971, DOI: **10.1021/jacs.4c11899**.
30 M. Umar, H. A. Aziz and M. S. Yusoff, *Waste Manag.*, 2010, **30**, 2113–2121.
31 S. O. Ganiyu, M. Zhou and C. A. Martínez-Huitle, *Appl. Catal., B*, 2018, **235**, 103–129.
32 S. Chen, S. Liang, R. Huang, M. Zhang, Y. Song, Y. Zhang, S. Tao, L. Yu and D. Deng, *Nat. Synth.*, 2024, **3**, 76–84.
33 H. Kojima, N. Nakatsubo, K. Kikuchi, S. Kawahara, Y. Kirino, H. Nagoshi, Y. Hirata and T. Nagano, *Anal. Chem.*, 1998, **70**, 2446–2453.
34 L. J. Ignarro, J. M. Fukuto, J. M. Griscavage, N. E. Rogers and R. E. Byrns, *Proc. Natl. Acad. Sci. U. S. A.*, 1993, **90**, 8103–8107.
35 X. Song, C. Basheer, Y. Xia and R. N. Zare, *Environ. Sci. Technol.*, 2024, **58**, 16196–16203.
36 J. Li, Y. Xia, X. Song, B. Chen and R. N. Zare, *Proc. Natl. Acad. Sci. U. S. A.*, 2024, **121**, e2318408121.